ADVANCED THERAPEUTICS
www.advtherap.com

Harnessing an Artificial Intelligence Platform to Dynamically Individualize Combination Therapy for Treating Colorectal Carcinoma in a Rat Model

Xianting Ding, Vincent H. S. Chang, Yulong Li, Xin Li, Hongquan Xu, Chih-Ming Ho, Dean Ho,* and Yun Yen**

Designing multi-drug regimens often involves target- and synergy prediction-based drug selection, and subsequent dose escalation to achieve the maximum tolerated dose (MTD) of each drug. This approach may improve efficacy, but not the optimal efficacy and often substantially increases toxicity. Drug interactions depend on many pathways in the omics networks and further complicate the design process. The virtually infinite drug–dose parameter space cannot be reconciled using conventional approaches, which are largely based on prediction. This barrier at least partially accounts for the low response rates that are observed with conventional mono- and combinatorial chemotherapy. A combination of nonstandard therapies for colorectal cancer (AGCH: adriamycin, gemcitabine, cisplatin, and herceptin) at ¼ MTD is used to treat the rats, the tumor response rates varied in a wide range. Some of the tumor response rates are close to that of control group. This work harnesses an artificial intelligence (AI) platform that is mechanism free and can dynamically optimize combinatorial therapy in rats. The individually optimized AGCH regimen reveal starkly different drug–dose parameters, which can converge each rat toward the same and low tumor response rate. Importantly, this AI-based drug–dose optimization technology is an actionable platform, which can achieve N-of-1 therapy.

1. Introduction

Colorectal carcinoma (CRC) is the third most common cancer in men (663 000 cases, 10.0% of all cancer cases) and the second most common cancer in women (571 000 cases, 9.4% of all cancer cases) worldwide.[1] The lifetime risk of developing CRC is ≈1 in 20 (5.1%).[2,3] Numerous cancer therapies such as 5-fluorouracil (5-FU), irinotecan, oxaliplatin, bevacizumab, cetuximab, and panitumumab, and the oral drug capecitabine have been effective against CRC. Several combinations of these drugs, such as FOLFOX (leucovorin, 5-FU, and oxaliplatin), FOLFIRI (leucovorin, 5-FU, and irinotecan), and XELOX (oxaliplatin and capecitabine), with or without a monoclonal antibody, have been reported to improve CRC treatment outcomes.[4–16] However, the efficacy of current chemotherapeutic agents against CRC has reached a plateau. The chemotherapy response rate is about 25%.[17] The 5-year survival rate of patients with advanced CRC has remained <8% due to the development of resistance to treatment.[18] With regard to more recently developed therapies, tyrosine kinase inhibitors can potentially avoid chemotherapy-induced cytotoxicity.[19] Targeted agents can potentially overcome chemotherapy resistance and enhance patient response localized or advanced cancer.[20] Despite their promising potential, these inhibitors have benefited only certain patient populations with CRC.[21–23] In this study, we tested a new combination of existing drugs for increasing response. The present study evaluated the CRC tumor response inhibitory effects of the four-drug combination (AGCH: adriamycin,

Prof. X. Ding, Y. Li, X. Li
Institute for Personalized Medicine, State Key Laboratory of Oncogenes and Related Genes of Biomedical Engineering School
Shanghai Jiao Tong University
Shanghai 200030, China
Dr. V. H. S. Chang
Department of Physiology, School of Medicine, College of Medicine
Taipei Medical University
Taipei 110 Taiwan

The ORCID identification number(s) for the author(s) of this article can be found under https://doi.org/10.1002/adtp.201900127

DOI: 10.1002/adtp.201900127

Dr. V. H. S. Chang, Prof. Y. Yen
The PhD Program for Translational Medicine, College of Medical Science and Technology
Taipei Medical University
Taipei 110, Taiwan
E-mail: yyen@tmu.edu.tw
Prof. H. Xu
Department of Statistics
University of California
Los Angeles, CA 90095, USA
Prof. C.-M. Ho
Department of Bioengineering, Henry Samueli School of Engineering and Applied Science
University of California
Los Angeles, CA 90095, USA
E-mail: chihming@g.ucla.edu

gemcitabine, cisplatin, and herceptin) in rat model. The four compounds are not typically used as monotherapies toward colorectal cancer, or in combination with other drugs. Among the four drugs, cisplatin, adriamycin, and gemcitabine are chemo agents. They target on TopoII and DNA replication enzyme. Herceptin is an antibody, which targets on EGFR receptor ERB2. Combinatorial application of these agents potentially exerted beneficial effects and promoted their anti-CRC efficacy.

In combinatorial therapy, simultaneously reconciling the drug and dose space is required. This is due to the fact that drug synergy is dose dependent and as such, delivering what are perceived to be suitable drugs at the wrong dose ratios can lead to suboptimal responses.[12–14,16,24–29] Promising strategies to design novel drug combinations have included pairwise drug predictions, systems biology-guided drug combination design, as well as ex vivo and disease modeling approaches, among others, in an effort to estimate how diseased systems will respond to multi-drug inputs.[29–37] Furthermore, delivering drugs that may have never been considered at the right dose ratios can lead to treatment responses that markedly exceed conventional regimens.[38–42] Optimizing both drug and dose at the same time, the search space is too large to be handled by the conventional high throughput technology. This insurmountable barrier at least partially accounts for the high incidence of drug trial failure and low response rates.[43,44]

In addition to the large drug–dose search space, the detailed mechanisms of drug–dose interacting with cellular omics and physiological functions present further challenges to identify the most potent regimen for patients. Hence, artificial intelligence (AI) is selected in this study for the reason that it is a mechanism-independent enabling technology to search and to optimize the desired outcomes by learning from a set of data. AI can be actionably executed to address disease heterogeneity, pharmacokinetics, co-morbidities, and rapid changes to patient physiology.[45–47] AI is an indication agnostic and model-free platform, which can rapidly and dynamically optimize treatment for the entire duration of care.

Prof. C.-M. Ho
Department of Mechanical and Aerospace Engineering, Henry Samueli School of Engineering and Applied Science
University of California
Los Angeles, CA 90095, USA
Prof. D. Ho
The N.1 Institute for Health (N.1)
National University of Singapore
Singapore 117456
E-mail: biedh@nus.edu.sg
Prof. D. Ho
Department of Biomedical Engineering, NUS Engineering
National University of Singapore
Singapore 117583
Prof. D. Ho
Department of Pharmacology, Yong Loo Lin School of Medicine
National University of Singapore
Singapore 117600
Prof. Y. Yen
Chemical Engineering, Division of Chemistry and Chemical Engineering
California Institute of Technology
California 91125 USA

The broader definition of AI, particularly in the context of medicine, is the use of large data sets to train algorithms to iteratively solve for constants in these algorithms that can mediate improved image recognition for diagnostics, as well as drug discovery and development.[25,48–53] With a few hundred experimental data points, we applied an artificial intelligence (AI)-based neural networks approach to correlate drug–dose inputs with phenotypic outputs (tumor burden, toxicity markers).[54] The phenotypic response surface (PRS) surprisingly has a very smooth landscape, which indicates that the efficacies/toxicities has a simple relationship with the therapeutic inputs.

It is very encouraging the AI platform leads to a smooth PRS. We further discovered that this PRS surface is governed by a quadratic algebraic series, which collectively mediates the actionability of this platform.[54] The quadratic algebraic polynomials can be expressed as follows.

$$R(C,t) = x_o + \Sigma x_i(t)\, c_i(t) + \Sigma y_{ii}(t)\, c_i(t)^2 + \Sigma z_{ij}(t)\, c_i(t)\, c_j(t) \quad (1)$$

where $c_i(t)$ and $c_j(t)$ are drug concentrations at time t. The coefficients, x_o, x_i, y_{ii}, and z_{ij}, define the interactions of drugs with both the molecular mechanisms (genetics, proteomics transcriptomics, and metabolomics, etc.) and unique physiological behavior (metabolism, immune system and pharmacokinetics, etc.) of a biological system ranging from cells, to animals, to patients.[46,55–58] PRS derived by the augmented AI technology has shown that the phenotypic response to drug administration can be represented quadratically. The discovery of the PRS correlation in turn eliminates the need for big data training sets, which is not feasible in clinical setting. Our AI-PRS platform is augmented in that it uses rapid experimental validation, and not in silico methods, for optimization.

Based on the PRS correlation, a rationally developed, small number of calibration assays (in vitro, preclinical, or human) can be used in concert for deterministically identifying these coefficients and immediately prescribing a globally optimal treatment course.[45,54,55,59,60] For example, in an in vitro search of potent drug–dose combinations from a pool of 14 drugs, Equation (1) has 120 coefficients. Instead of carrying out 6 billion high throughput tests, 120 experiments can tell us the optimized regimens ranked by efficacy.[55] In in vivo setting, only very small number of data points are available, especially in the case of personalized therapy. In other words, large amount training data is not possible for in vivo test. The AI-PRS equation enables immediate implementation of the optimized drug doses at a given time, t, and dynamically re-optimizes these doses during treatment to adjust for mechanistic (e.g., genomics, proteomics, transcriptomics), physiological, and treatment regimen changes in personalized medicine.[46,57] As AI-PRS is a model-free approach, the implementation is agnostic to the class of drugs used or indication being treated, and has been validated in multiple disease indications ranging from cancers,[57] infectious diseases[55,56] to immunosuppression.[30] Therefore, the PRS correlation serves as a hallmark for the actionability of our platform, which has been validated in cell line, preclinical, and clinical tests.[38,46,54–58,61,62]

The aberrant pathways in diseased cells will make the omics networks depart from their normal functions, which will propagate to organs and to entire body. Identifying the disease mechanisms and tracing their interactions with cellular and

physiological functions are overwhelmingly complex. After drug being applied, how the drugs interplay with cascade cellular and physiological mechanisms to reach therapeutic purposes is at least equally complex. We have applied the AI-PRS for indications such as cancer,[57] infectious disease,[56] and organ transplant.[46] In this work, we use the platform for studying optimized combinatorial therapy for solid tumor in genetically homogeneous rat and cancel cell line, such that the effects of physiology of individual rat can be examined.

Using the PRS augmented AI platform, a novel combination therapy (AGCH: adriamycin, gemcitabine, cisplatin, and herceptin), was dynamically optimized to increase the treatment response rate using rat models (**Figure 1**). Of note, these four compounds are not typically used as monotherapies toward CRC, or in combination with other drugs. AI agnostically optimizes the combination of these four drugs to reconcile the best dosages modulated over time, independent of target or mechanistic biology. Following the initial administration of AGCH at ¼ maximum tolerated dose (MTD) of each drug to each rat, which also served as the calibration period for the PRS coefficients, a substantial level of variability was observed between the treated rats during the initial calibration period, even when using the genetically homogeneous rats and cancer cell line for the study. Upon PRS implementation, each rat was treated by the individually optimized regimen (IOR). The tumor response in each rat was actionably converged such that all rats responded to treatment. Importantly, all rat tumors collapsed in a uniform fashion to reveal a universally potent and collective treatment response. In order to achieve this outcome, this work demonstrates the substantial changes to drug dose and individualized dose modulation that are required for each rat. AI-PRS successfully reconciled these differences to result in collective agnostic optimization of first-order, second-order, and drug–drug interaction terms of the PRS equation that resulted in optimized treatment responses for all rats, despite subject-specific drug antagonism. In effect, PRS augmented AI platform successfully uncovered the foundation for why population-averaged drug administration results in low response rates, and actionably overcame this barrier to mediate optimized multi-drug treatment.

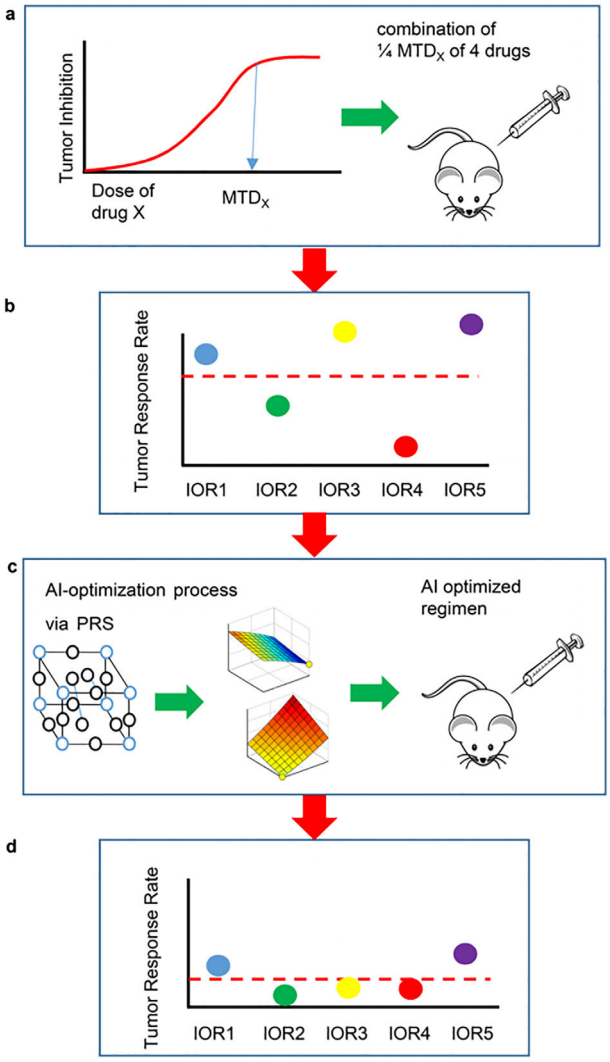

Figure 1. Augmented artificial intelligence-guided optimization of individualized combination therapy. a) Based on dose response curves of drug x, the calibration regimen (CR) dose of drug x are determined. All rats are treated with the CR on day 1 and day 7. b) The highly variable tumor response rates of all rats are measured and correlated with the corresponding drug dose inputs. c) Based on the drug–dose values and the tumor response rate of individual rat, the phenotypic response surface (PRS) platform was applied to obtain the individually optimized regimen (IOR) for each rat. d) The subject-specific IOR regimen is subsequently administered on day 14 and day 24 to comprehensively converge to the best tumor response rate.

2. Results

2.1. Calibration: ¼ Maximum Tolerated Dose Regimen and Individually Optimized Regimen

In this study, a rat model (Crl:NIH-*Foxn1*^{rnu}, Charles River) was used to test a new antitumor regimen (AGCH: cisplatin, adriamycin, herceptin, and gemcitabine) to treat CRC. Each rat was inoculated subcutaneously at the rear right flank with HT-29 colon cancer cells (1×10^6) in 0.1 mL of PBS.[63] The tumor size served as the primary efficacy indicator.

Based on the MTDs obtained from the literature (Table S1, Supporting Information), the ¼ MTD regimen was developed by combining the ¼ MTD of each of the four drugs. The ¼ MTD regimen was as follows: cisplatin, 1.5 mg kg^{-1}; adriamycin, 1.5 mg kg^{-1}; herceptin, 82.7 mg kg^{-1}; and gemcitabine, 30.0 mg kg^{-1}. The IOR was determined using PRS technology for each rat according to the protocol described in the Section 4. The weight and dosing level of each rat in IOR group are listed in Table S2, Supporting Information.

The study included two groups of rats. The three rats in the control group (C1–C3) were treated with the same volume (0.1 mL) of phosphate-buffered saline (PBS). The five rats in the IOR group (IOR1–IOR5) were treated with ¼ MTD doses for each drug in the morning of day 1 and day 7. The five rats were treated by IOR in the morning of day 14 and 24. The tumor sizes were measured in the afternoon of every day (Figure S1, Supporting Information).

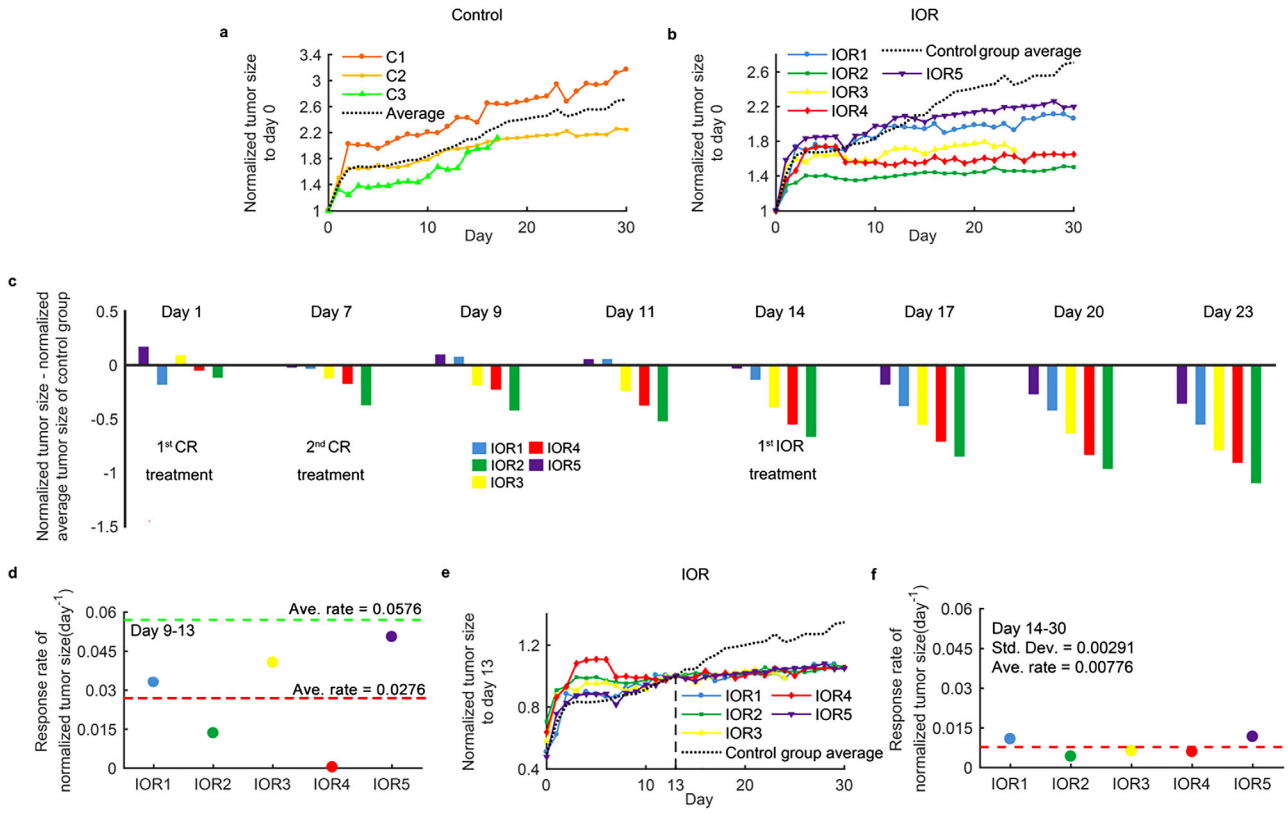

Figure 2. Harnessing augmented artificial intelligence to individually optimize dynamic combination therapy. a) The tumor responses of the control group during days 1–3 are shown ($n = 3$). No apparent efficacy is observed. Tumor sizes were normalized to the tumor size of individual rats measured at day 0. b) The CR regimen was applied on day 1 and day 7 and the normalized tumor size is shown ($n = 5$). Tumor sizes were normalized to the tumor size of individual rats measured at day 0. The IOR regimen was applied on day 14 and the tumor sizes were normalized to the tumor size of the individual rat measured at day 0 ($n = 5$). c) A waterfall plot based on the normalized tumor size deducted by the normalized average tumor size of the control group is shown for IOR1, IOR2, IOR3, IOR4, and IOR5. d) The response rate based on the normalized tumor size for all five subjects from days 9–13 is shown (average rate = 0.0276, SD = 0.0183). The green dashed line is the averaged response rate of the control group (average rate = 0.0576, SD = 0.0204) e) The tumor sizes normalized to the tumor size of the individual rat measured at day 13 are shown for the IOR group ($n = 5$). The control group average tumor size during the course of treatment is shown. f) The response rate based on the normalized tumor size for all five subjects from days 14–30 is shown (average rate = 0.00776, SD = 0.00291).

2.2. Individually Optimized Regimens Markedly Enhance Tumor Treatment Response

The normalized tumor size is the tumor size of a rat measured at a specific day of interest divided by the tumor size at day 0 (Table S2, Supporting Information). To provide more insight into the high degree of variability in PBS treatment response between rats C1 and C3 during the 30-day treatment period that subsequently required management by PRS, tumor response normalized to the tumor size of each rat at day 0 were plotted (**Figure 2**a). During days 0–3, the tumor response increased in a linear fashion with time. During days 3–9, tumor experienced regress (C1) and slow response (C2 and C3). From days 9–30, tumors of rats C1 and rats C2 have linearly response rate. Rat C3 had much faster tumor response rate after day 9 and started to fizzle on day 18.

The normalized tumor sizes of rats IOR1–5 and the average response of the control group were plotted (Figure 2b). These rats also exhibited highly diverse responses while under treatment with ¼ MTD regimens. During days 0–3, tumor response increased in a linear fashion. During days 3–9, as previously observed with rats C1–3, tumor response exhibited an unsteady/high variable state, where tumor response occurred between days 3 and 5, and regression was clearly observed for rats IOR1, IOR2, and IOR4 between days 5 and 9 (Figure 2b). During days 9–13, tumor responses resumed with an average normalized tumor response rate of 0.0276/day (SD = 0.0183). Among the five rats, only rat IOR4 had a clearly favorable response to the ¼ MTD regimen (Figure 2d). A waterfall plot was analyzed to demonstrate the variability in each subject's response to ¼ MTD treatment, and the resulting use of the IOR regimen to optimize the time-dependent, dose-dependent, and subject-specific responses to treatment efficacy (Figure 2c).[64] In the waterfall figure, the normalized averaged tumor size of the control group was used as the reference. In this plot, IOR administration results in a substantial increase in efficacy.

It is widely recognized that combination chemotherapy results in highly variable treatment outcomes between patients and response rates of ≈25%.[65] The inability to pinpoint optimized doses in the combination to accommodate genetics related human heterogeneity and patient-specific physiological responses

to therapy combination results in implicitly suboptimal treatment efficacy and could be the reason for low response rate under ¼ MTD treatment (Figure 2d). Among the five rats, the response rates of Rats 3 and 5 are close to that of the control group (green dashed line). Only IOR4 has the best response rate. Remarkably, upon IOR implementation, the AI-PRS-derived optimal doses for each rat resulted in all IOR rats responding to treatment with all rats collapsing toward a uniform normalized tumor response rate (Figure 2e). Furthermore, the rats uniformly converged toward the average tumor response rate of 0.00776/day (SD = 0.00291), which was similar to the response rate of IOR4, the best among all five rats under ¼ MTD treatment (Figure 2f). The averaged tumor response rate of the IOR group from day 14 to day 30 was about 13.5% of the tumor response rate of the control group from day 9 to day 30 (Figure 2a,f).

2.3. Dynamic Responses of the Phenotypic Response Surface

To demonstrate how dose ratios can substantially affect the subject-specific nature at any given time during treatment, PRS drug interaction surfaces based on the prospective treatment of the IOR cohort were plotted. For a four-drug regimen, six drug–drug interaction surfaces are created, with the horizontal axes showing the drug doses and the vertical axis representing the normalized tumor size. As such, the PRS visualizes tumor size variations as they correlate with drug doses based on experimental validation, not estimation or prediction. Importantly, this plot implicitly represents the integration of disease mechanisms (e.g., genomics, proteomics, transcriptomes, etc.) as well as physiology and drug behavior for a specific subject. The PRS plots continuously varied during the 3 days following ¼ MTD regimen administrations on day 7. These surfaces can change rapidly during treatment and PRS-mediated identification of these surfaces as they undergo dynamic changes during the course enables continuous optimization during the course of treatment (Video S1, Supporting Information).

The PRS plots for each of the five IOR rats at day 13 are shown, with the yellow markers denoting the IOR that was administrated on day 14 (**Figure 3** and Video S1, Supporting Information). From these surfaces, the PRSs of Rats 1, 2, and 4 are different but have similar patterns. However, the PRSs of Rat 3 are similar to those of Rats 1, 2, and 4, but adriamycin–cisplatin interaction is different from that of Rats 1, 2, and 4. Rat 5 has different patterns from that of the other four rats. The tumor response rates of Rats 3, 5 are higher than the response rates of the other three rats in IOR group (Figure 2d).

2.4. Linear, Quadratic, and Drug–Drug Interaction Terms of the AI-PRS Equation

The phenotypic outputs were obtained based on the PRS platform by optimizing the drug and dose inputs according to Equation (1), with one coefficient, x_0, and 14 terms for a four-drug combination. Not all of the terms contribute to tumor response at all the time, and the drug–drug interactions terms can be either synergistic or antagonistic. However, all of these terms must be considered in order to achieve global optimization, and at least 15 experimental assays are required to solve for these terms. In experimental terms, this means that predictive analysis (e.g., drug–drug interactions) cannot substitute experimental validation. Most importantly, PRS can guide the search of the IOR doses of the drugs and eventually lead the intricate balances of 15 terms to the most desired tumor responses for all the tested subjects. Using AI-PRS platform to identify this set of 15 coefficients and terms is the foundation of deterministic optimization during the dynamic treatment regimen.

Each term in Equation (1) consists of a coefficient multiplied by the concentrations c_i, c_i^2, or $c_i c_j$. The dose of each drug is an independent variable and could be freely adjusted during the course of the study. The values of coefficients x_i, γ_{ii}, and z_{ij} reflect the changes in the phenotypic outputs (e.g., tumor size), which are a function of subject genomics, proteomics and metabolomics, and other omics mechanisms, as well as drug–physiology interactions (Table S3, Supporting Information). Hence, these coefficients are cross-correlated and dependent on time and the physiological conditions of each test subject. Terms associated with c_i are contributed by the linear drug effects on tumor response. Terms associated with c_i^2 are contributed by the quadratic drug effects on tumor response. Terms associated with $c_i c_j$ are contributed by the drug–drug interaction (synergistic or antagonistic) effects on tumor response. The actual increase or decrease in tumor size is associated with the sum of all 15 products of coefficients and concentrations. Therefore, synergism and antagonism, which are often represented by drug–drug interactions, constitute only a portion of the factors that impact tumor response.

2.5. The Drug–Drug Interactions that Dictate Synergism and Antagonism are Time Dependent

By integrating each term in Equation (1) from day 0 to day 13 and normalizing to the tumor size at day 0, the sum is the normalized tumor size at day 13. From day 0 to day 13, rats IOR1–IOR5 were given the ¼ MTD regimen. The dynamic behavior of the drug–drug interaction terms and their impact on tumor size were analyzed for day 7 to day 13 (**Figure 4**). Day 7 was the second treatment of ¼ MTD regimen. The synergism or antagonism between two drugs depends on multiple factors including the specific subject being treated. For the drug–drug interaction term, if the value is negative and will reduce the tumor size, this value represents drug synergy. If the value is positive, these two drugs will be antagonistic. For the same rat, the drug–drug interactions are not all synergetic (negative values) or all antagonistic (positive values). The magnitudes of the drug–drug interactions became pronounced except IOR 3 after day 9. The tumor response rate of each rat from day 9 to day 13 was almost constant (Figure 1d).

2.6. Tumor Response Contributed by the Linear, Quadratic, and Drug–Drug Interaction Terms

All 15 terms of IOR1 (**Figure 5**a), IOR2 (Figure 5b), IOR3 (Figure 5c), IOR4 (Figure 5d), and IOR5 (Figure 5e), are plotted

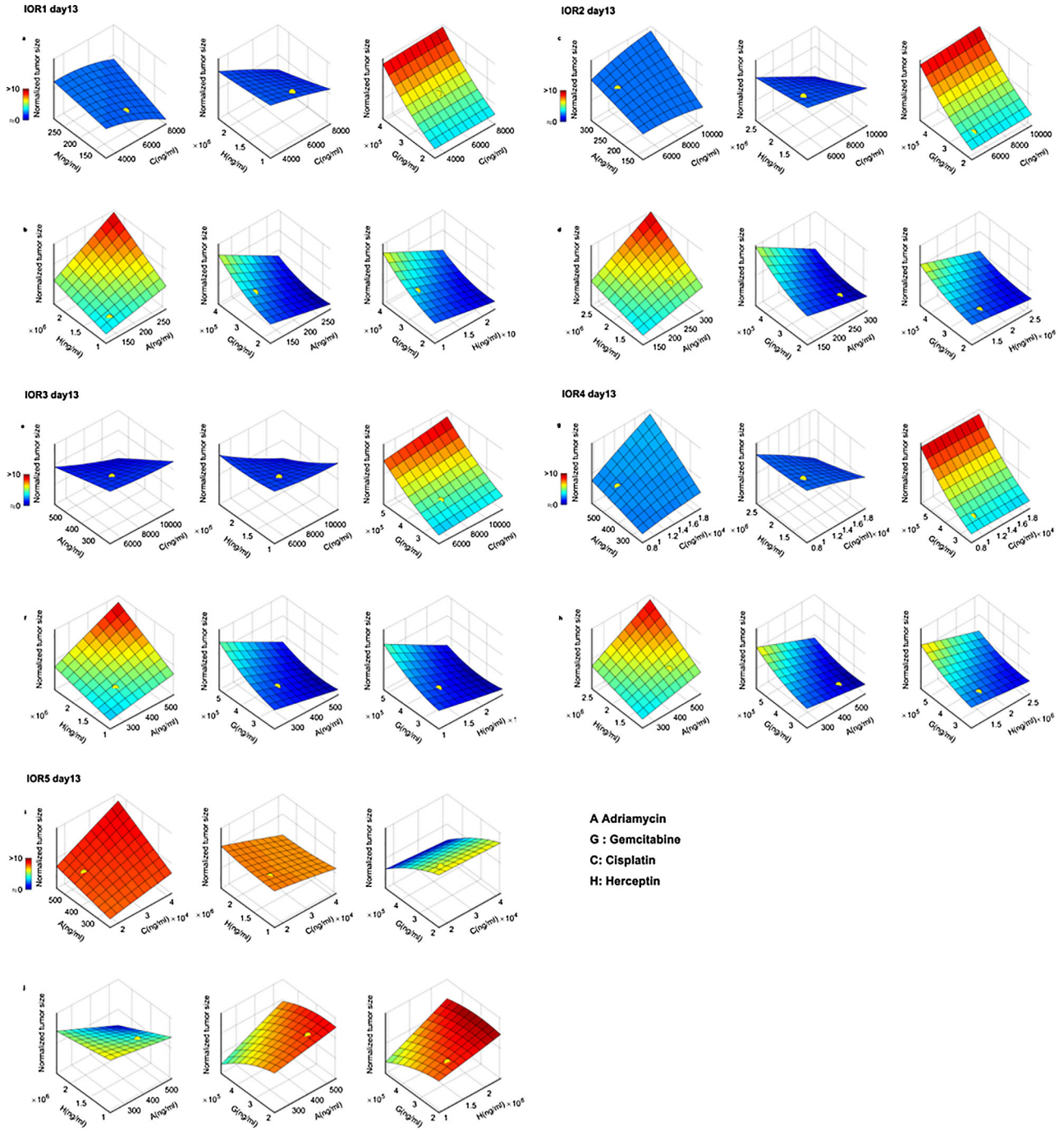

Figure 3. Dynamic responses of phenotypic response surface (PRS). Optimized drug–drug interactions of IOR1, IOR2, IOR3, IOR4, and IOR5 on day 13 are shown. Optimal dosing parameters are indicated by a yellow marker. a) IOR1: Optimized drug interaction PRS plots for adriamycin–cisplatin, herceptin–cisplatin, and gemcitabine–cisplatin are shown. b) IOR1: Optimized drug interaction PRS plots for herceptin–adriamycin, gemcitabine–adriamycin, and gemcitabine–herceptin are shown. c) IOR2: Optimized drug interaction PRS plots for adriamycin–cisplatin, herceptin–cisplatin, and gemcitabine–cisplatin are shown. d) IOR2: Optimized drug interaction PRS plots for herceptin–adriamycin, gemcitabine–adriamycin, and gemcitabine–herceptin are shown. e) IOR3: Optimized drug interaction PRS plots for adriamycin–cisplatin, herceptin–cisplatin, and gemcitabine–cisplatin are shown. f) IOR3: Optimized drug interaction PRS plots for herceptin–adriamycin, gemcitabine–adriamycin, and gemcitabine–herceptin are shown. g) IOR4: Optimized drug interaction PRS plots for adriamycin–cisplatin, herceptin–cisplatin, and gemcitabine–cisplatin are shown. h) IOR4: Optimized drug interaction PRS plots for herceptin–adriamycin, gemcitabine–adriamycin, and gemcitabine–herceptin are shown. i) IOR5: Optimized drug interaction PRS plots for adriamycin–cisplatin, herceptin–cisplatin, and gemcitabine–cisplatin are shown. j) IOR5: Optimized drug interaction PRS plots for herceptin–adriamycin, gemcitabine–adriamycin, and gemcitabine–herceptin are shown.

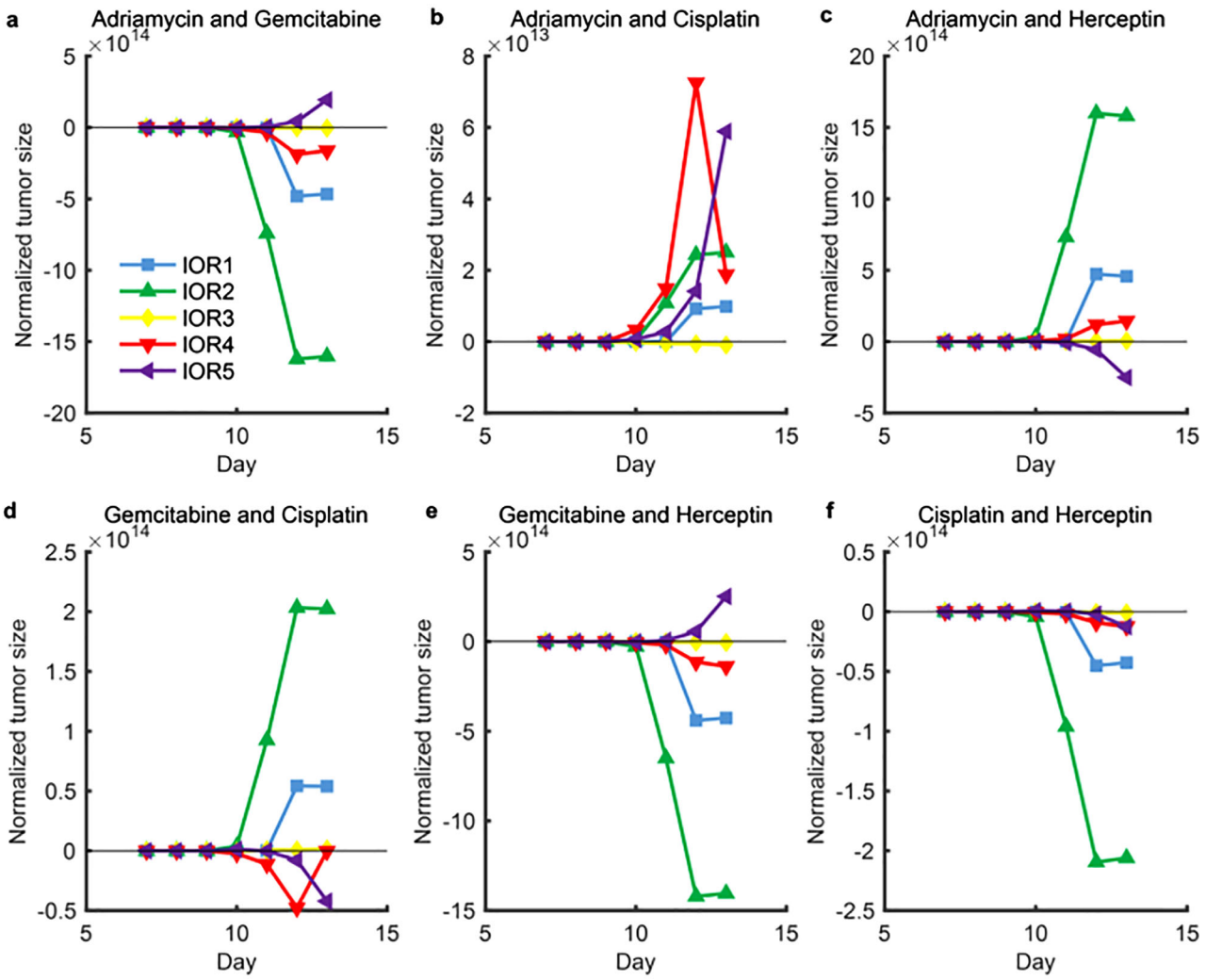

Figure 4. The tumor treatment response is mediated time-dependent drug interaction terms. Normalized tumor sizes are plotted against drug–drug interaction terms as a function of time for IOR1 to IOR5. A shift between drug synergism and antagonism is observed over time, demonstrating the need for dynamic modulation of combination therapy to maintain optimized treatment outcomes. a) The impact of adriamycin–gemcitabine interactions on the normalized tumor size over time is shown. b) The impact of adriamycin–cisplatin interactions on the normalized tumor size over time is shown. c) The impact of adriamycin–herceptin interactions on the normalized tumor size over time is shown. d) The impact of gemcitabine–cisplatin interactions on the normalized tumor size over time is shown. e) The impact of gemcitabine–herceptin interactions on the normalized tumor size over time is shown. f) The impact of cisplatin–herceptin interactions on the normalized tumor size over time is shown.

where $i = 1$, 2, 3, and 4 for adriamycin, gemcitabine, cisplatin, and herceptin, respectively. All 15 PRS terms are either positive or negative, with similar magnitudes, so that the predictive analysis only based on drug–drug interaction terms cannot give a correct population-wide estimation of the resulting efficacy and or toxicity. At day 13, the linear terms have no contributions to the tumor response. Taking z_{12} as an example, a negative reading indicates synergism between drugs 1 and 2 at day 13 for rat IOR1 (Figure 5a). Conversely, z_{12} is antagonism in IOR5 (Figure 5e). Furthermore, the patterns of the 15 PRS terms (coefficients multiplied by the drug doses) of IOR1, 2, 3, and 4 are similar. The signs of these terms of IOR5 are opposite to those in other rats. The PRS analysis of terms revealed the substantial variability in the contribution of their combinations toward tumor treatment response between the subjects. Nonetheless, augmented AI-PRS implementation agnostically minimized the sum of all 15 terms to optimize efficacy across all subjects.

2.7. Tumor Response Contributed by the Sums of Linear, Quadratic, and Drug–Drug Interaction Terms

The sum of the linear, quadratic, and drug–drug interaction terms for each rat was plotted (**Figure 6**). Prior to day 14, the rats were treated by ¼ MTD regimen. As previously established, the treatment response is governed by all 15 terms of the four-drug combinatorial regimen. Substantial variability in the contribution of these terms toward tumor treatment response was observed for days 6 and 7, for each subject. For example, the sum of the linear terms contributed more toward tumor treatment

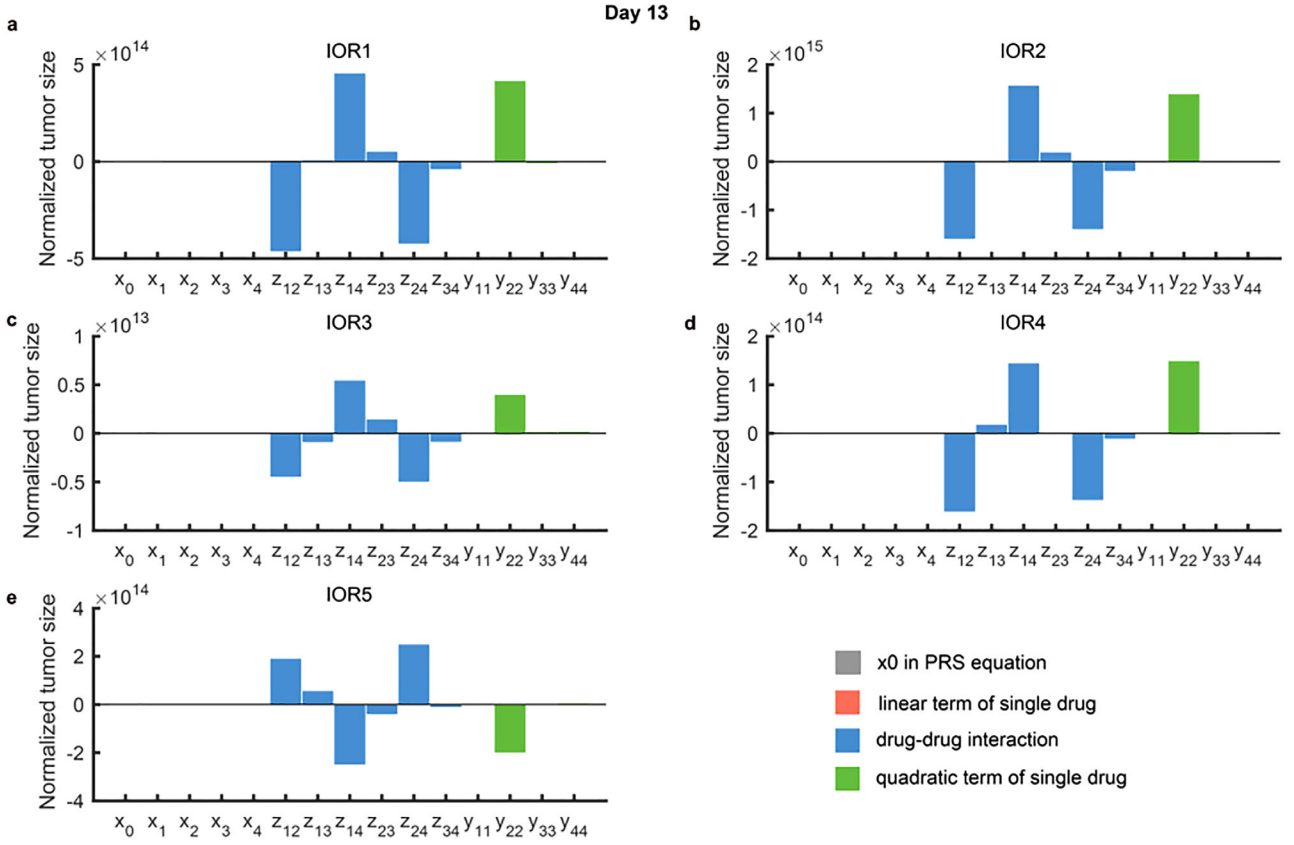

Figure 5. Linear, quadratic, and drug interaction terms govern tumor treatment efficacy. The 15 outlined terms identify the linear relation of the drug dose, the quadratic relation of the drug dose, as well as drug–drug interactions. The numerical subscripts serve as drug identifiers: 1: adriamycin, 2: gemcitabine, 3: cisplatin, 4: herceptin. a) IOR1 terms are shown for day 13. b) IOR2 terms are shown for day 13. c) IOR3 terms are shown for day 13. d) IOR4 terms are shown for day 13. e) IOR5 terms are shown for day 13.

response during day 6 for IOR2, IOR3, and IOR5 compared to IOR1 and IOR4. Day 7 was the second treatment with ¼ MTD regimen. After day 7, the tumor responses of all rats depend on the sum of the quadratic and drug–drug interaction terms. The signs of the sum of quadratic and drug–drug interactions terms are always opposite. The signs may switch between day 8 and day 10. Hence, the synergism and antagonism among drugs are dynamic and not a universal property of drug pairs. During days 11–13, the sum of drug–drug interaction terms of IOR1, IOR2, IOR3, and IOR4 are all negative (synergetic). Only IOR 5 had antagonistic drug–drug interactions and also has the highest tumor response rate (Figure 2d).

2.8. Safety Study

To verify the safety of the IOR therapy approach used in this study, we investigated two important biomarkers, namely the blood neutrophil levels and the serum alanine aminotransferase (ALT) levels after IOR administration. After the third treatment (day 21), the neutrophil levels increased significantly in the IOR compared to those in the control group. However, after the fourth treatment (day 31), no significant differences were observed in the neutrophil levels of the two groups (Figure S3a, Supporting Information). Furthermore, the serum ALT levels were monitored after the third treatment to assess liver toxicity. The control and IOR showed similar variations in ALT levels (Figure S3b, Supporting Information). A correlation of the tumor size on day 21 normalized to day 13 with the serum ALT levels for the control and IOR cohorts further revealed no apparent toxicity of the AGCH combination (Figure S3c, Supporting Information). As such, the rats treated by IOR did not exhibit any apparent liver toxicity. The substantially reduced tumor sizes coupled with unimpaired liver function and absence of prolonged neutrophil level changes suggested that the IOR was simultaneously efficacious and well tolerated (Figure S3c, Supporting Information).

3. Discussion

Combinatory therapy is a mainstay for treating a variety of diseases. However, it is an insurmountable challenge to trace the mechanistic interactions among the drug–dose combinations with the cellular omics and physiological functions. Therefore, MTD is the common practice for determining the doses of drug combination and usually ends with high toxicity and suboptimal efficacy. We harnessed an AI neural networks platform, which bypassed the big parameter space and revealed that the subject body response to the therapeutic inputs is a smooth surface.

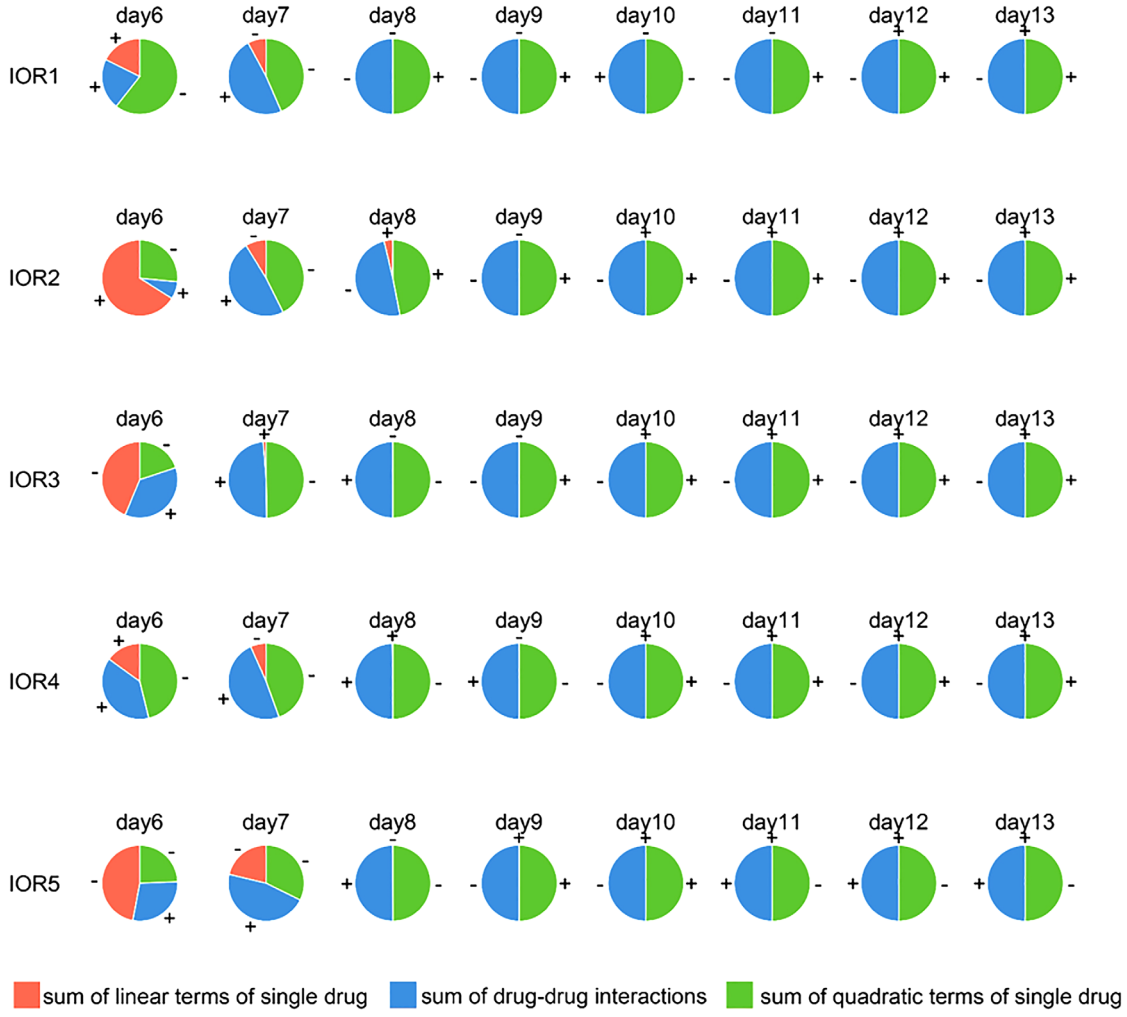

Figure 6. Minimizing the sum of the linear, quadratic, and drug interaction terms optimizes combination therapy. The contributions to the tumor size response based on the sum of the linear terms, quadratic terms, and the drug–drug interaction terms are plotted for IOR1, IOR2, IOR3, IOR4, and IOR5 as a function of time.

Furthermore, we discovered that the smooth PRS can be represented by a quadratic algebraic equation (Equation (1)), which does not need a large number of data to train the neural networks. Only a small set of orthogonally designed assays[66] can solve the coefficients of PRS equation and dynamically optimize individualized or population-averaged combinatorial therapy. The PRS correlation augmented by AI is agnostic to indications, independent of disease mechanisms and accommodates the unique physiology of the treated subject.[38,46,54–56]

In this study, we are interested in exploring whether systemic diversity exists in genomic homogeneous rat with colon cancer induced by genomic homogeneous CRC cell line. In addition, we want to demonstrate that PRS platform can individually optimize the combinatorial regimen for each rat with systemic diversities. Five rats (Crl: NIH-*Foxn1*^{rnu}, Charles River) were inoculated with HT-29 colon cancer cells. Conventional combination therapy is typically designed by selecting drugs to simultaneously address multiple aberrant targets and is believed to better mediate treatment outcomes compared to monotherapy. Unfortunately, response rates of combinatorial chemotherapy for oncology (e.g., gastrointestinal) have been only ≈25%.[65] When the five subjects are treated by AGCH regimen at the same calibration regimen, ¼ MTD, the tumor response rates of the subjects were highly variable. In fact, only 1 out from 5 rats, IOR4, exhibited a favorable tumor treatment response (Figure 2d). Systemic diversity does appear despite the rats and the cancer cell line being genetically homogeneous. We actionably captured the optimal drug–dose parameters required to continuously identify the individually optimal regimen that ultimately leads to a uniform collapse of the tumor size across the full IOR cohort (Figure 2e,f). It is interesting to note that many drugs of IOR regimen had doses as low as 20% of the ¼ MTD dose while the regimen had optimal efficacy (Table S4, Supporting Information).

In addition, when the IOR doses of same drug were averaged across different rats, the population-averaged IOR regimen is about 0.65 × (¼ MTD) (Table S4, Supporting Information). In order words, population-averaged IOR treatment ignoring the systematic diversities will not achieve uniformly low tumor response rate. Most importantly, the features of all IORs having very different dosing patterns (Table S4, Supporting Information)

demonstrate that simply increasing the number of test subjects may not serve as an actionable strategy to improve the population-wide treatment response. The nonlinear quadratic and interaction terms play major roles in determining the performance in the combinatorial regimen (Figure 6). This fact dictates that the conventional additive approach of developing drug combination deems to have low successful rate.

Synergism is generally assumed to be universal among the population and is the reason for combinatorial therapy being more effective than monotherapy. However, AI-PRS optimization showed that synergism/antagonism is not universal across the subject population (Figures 5 and 6). Interesting enough, the combined drug–drug interactions of IOR1, 2, 3, and 4 were synergetic, but IOR5 was antagonistic (Figure 6). Furthermore, IOR5 has the tumor response rate that is close to that in the control group (Figure 2d). IOR 3 also had high tumor response rate about the same as that of the control group (Figure 1d) as all the drug–drug interactions of IOR3 are close to zero from day 7 to day 13 (Figure 4).

During both ¼ MTD and IOR treatments (Figures 3, 4 and 6), not only is drug synergy subject specific at a given point in time, it can also change over time in the same subject (Figure 6). We have shown this to be true in a prospective clinical immunosuppression study as well.[54] Furthermore, AI-PRS platform showed that minimizing the sum of the experimentally defined linear, interaction, and quadratic terms that defined the drug combination, in a continuous fashion, was required for dynamic global optimization. Hence, using AI-PRS to dynamically reconcile challenges such as dose and time dependence, as well as subject-specific physiology played a major role in determining the optimal composition of combinatorial therapy.

In fact, the systemic diversities do develop from the genetically homogeneous as evident by each rat having very different dosing patterns. Nevertheless, the PRS-platform-derived IOR can converge all the rats to have uniform tumor response. This augmented AI-PRS platform is model independent, and can be applied toward virtually all classes of drugs, having been previously validated for indications ranging from infectious diseases to clinical immunosuppression and regenerative medicine.[25,38,48–52] Future studies harness this platform to agnostically design novel drug combinations for subsequent individualization. In summary, augmented AI-PRS successfully reconciled a highly dynamic and individualized parameter space, leading to uniformly enhanced therapeutic response rates.

The primary objective of this work was not to harness AI to optimize drug selection. We have recently achieved this in previous publication.[67] The objective of this study was to demonstrate that: 1) dosing alone can be the difference between efficacy and no efficacy individuals between the same diseased model animals, and 2) dynamic dosing is an important element of sustained optimization in oncology treatment.[57] Conventional combination therapy design is based on perceived drug interactions and the objective of achieving drug synergy. This work further shows that this is a dynamic process, and is also dose dependent. Hence, this study is not seeking to implement the four-drug combo necessarily as a new standard combination. Instead, it demonstrates that fixed combination design and treatment based on purely mechanistic or synergy-driven factors is not sufficient to drive sustained treatment response.

4. Experimental Section

4.1. Rat Model

Ten rats (Crl:NIH-*Foxn1*^{rnu}, Charles River) were randomly distributed into two groups, the control group (C1,C2, C3, C4, C5) and IOR group (IOR1, IOR2, IOR3, IOR4, IOR5). Each rat was inoculated subcutaneously at the rear right flank with HT-29 colon cancer cells (1×10^6) in 0.1 mL of PBS to induce tumor formation according to an established protocol.[63] 3 weeks after tumor inoculation (designated as day 0), C4 and C5 were removed from the study due to early mortality unrelated to treatment. Note that the nude rats were purchased from Charles Rivers and shipped oversea. After such a long travel with shipping stress, two of the immune incompetent rats were weak and died several days after arrival. The IOR group received four treatments on day1, day7, day14, and day 24 (Table S2, Supporting Information). On day 1 and day 7, the IOR group was treated with the ¼ MTD regimen, which consisted of 1.5 mg kg^{-1} cisplatin, 1.5 mg kg^{-1} adriamycin, 82.7 mg kg^{-1} herceptin, and 30.0 mg kg^{-1} gemcitabine (Sigma-Aldrich, Tables S1 and S2, Supporting Information). The data obtained from the rats in control group (solvent-containing group) were used as baseline/background reference for deduction. The data obtained from experimental rats subtracted the baseline reference will then be used for further analysis. The tumor size was measured via optical Vernier. The tumor size and drug plasma concentration were measured in the first 64 h (Figure S4, Supporting Information) and every day for the first seven days (Figure S5, Supporting Information). On day 14 and day 24, each rat in the IOR group was treated with the IOR, which was determined by the PRS platform with serum drug doses and tumor sizes measured from day 1 to day13 (IOR1 shown in Table S5, Supporting Information). The tumor sizes for all of the rats were continuously monitored until day 30 (Figure 1a,b).

4.2. Individually Optimized Regimen Determined by PRS Platform

According to the PRS equation (Equation (1)), a minimum of 15 tests with different drug–dose ratios were needed to determine the 15 coefficients. During the first 13 days, all of the five IOR rats were treated with the ¼ MTD regimen. Based on the area under the cure of drug plasma levels and corresponding tumor sizes for each rat (Figure S6a–d, Supporting Information) and the measured tumor sizes (Figure S6e, Supporting Information), 15 data sets were generated from the 13 day's measurements with the help of interpolation. The information was used to determine the PRS coefficients for all IOR rats (Table S3, Supporting Information). After the coefficients of PRS equation being determined, the IOR doses administered on day 14 day 24 of the 5 rats that mediate optimal tumor response were listed (Table S2, Supporting Information). The tumor sizes of the IOR group were recorded until day 30 (Figure 1).

The computer codes used to determine the coefficients of the quadratic algebraic equation for fitting the PRS surface are available in MATLAB.

4.3. Safety Study

Blood samples were collected in 10% heparin from the retro-orbital vein and diluted in an equal volume of PBS containing 0.5% bovine serum albumin (BSA). Neutrophils were washed in PBS containing 0.5% BSA, counted, and re-suspended using an IDEXX ProCyte Dx hematology analyzer (IDEXX Laboratories Inc., Westbrook, ME, USA), according to the manufacturer's protocol (Figure S3, Supporting Information).

4.4. Statistical Analysis

The IOR cohort was statistically examined using nonlinear least-squares regression. MATLAB software was applied to examine the statistics using

the fitnlm function. The results of the statistical analysis of rat IOR4 were discussed and plotted in Figure S7, Supporting Information. The computer codes used for the statistical analysis are available in MATLAB.

Supporting Information

Supporting Information is available from the Wiley Online Library or from the author.

Acknowledgements

The authors gratefully thank Prof. Vivian Y. Chang and Prof. Kuan Wang at Taipei Medical University for helpful discussions. The authors gratefully thank Dr. Bingsen Zhou and Ms. Tiffany Lin at City of Hope for cell culture studies. X.D. and Y.L. acknowledge support from Shanghai Municipal Science and Technology Project (17DZ2203400) and State key research and development plan (2017YFC0107603 and 2017ZX10203205-006-002). V.H.S.C. and Y.Y. acknowledge support from Sino-American Cancer Foundation. C.-M.H. acknowledges support from endowment fund of Ben Rich-Lockheed Martin professorship. D.H. gratefully acknowledges support from a Ministry of Education Tier 1 FRC Grant, Singapore Ministry of Health's National Medical Research Council under its Open Fund-Large Collaborative Grant ("OF-LCG") (MOH-OFLCG18May-0003), National Institutes of Health grant R21DK116140, Wallace H. Coulter Foundation, and startup funds from the National University of Singapore. This study is partially supported by the Health and welfare surcharge of tobacco products grant (Grant Numbers: MOHW108-TDU-B-212-124014, MOHW108-TDU-B-212-124026 and MOHW108-TDU-B-212-124020) and Ministry of Education (MOE) in Taiwan. The animal studies reported this manuscript were conducted in accordance with the relevant ethical guidelines in the United States of America.

Conflict of Interest

X.D. and C.-M.H. are inventors on pending and issued patents pertaining to patents (International Patent Application Serial No. PCT/US2014/012111 and PCT/US2015/058892) covering the technology described herein. C.-M. H. is a co-inventor of pending patent WO2015017449. D.H. and C.M.H. are co-inventors of patents that also cover the technology described herein (US20170177834 and WO2016149529A1).

Author Contributions

X.D., V.H.S.C., and Y.L. contributed equally to this work. X.D. and V.H.S.C. performed the preclinical experiments. X.D., H. X., and Y.L. performed the prospective PRS augmented AI optimization. X.D., Y.L., X.L., C.-M.H., D.H., and Y.Y. performed the PRS augmented AI analysis. X.D., Y.L., C.-M.H., D.H., and Y.Y. wrote and edited the paper.

Keywords

artificial intelligence medicine, colorectal carcinoma, personalized medicine, rats

Received: July 1, 2019
Revised: September 16, 2019
Published online:

[1] J. Ferlay, I. Soerjomataram, R. Dikshit, S. Eser, C. Mathers, M. Rebelo, D. M. Parkin, D. Forman, F. Bray, *Int. J. Cancer* **2015**, *136*, E359.
[2] A. Jemal, R. Siegel, J. Q. Xu, E. Ward, *Ca-Cancer J. Clin.* **2010**, *60*, 277.
[3] M. Bretthauer, *Best Pract. Res., Clin. Gastroenterol.* **2010**, *24*, 417.
[4] R. G. Amado, M. Wolf, M. Peeters, E. Van Cutsem, S. Siena, D. J. Freeman, T. Juan, R. Sikorski, S. Suggs, R. Radinsky, S. D. Patterson, D. D. Chang, *J. Clin. Oncol.* **2008**, *26*, 1626.
[5] A. de Gramont, A. Figer, M. Seymour, M. Homerin, A. Hmissi, J. Cassidy, C. Boni, H. Cortes-Funes, A. Cervantes, G. Freyer, D. Papamichael, N. Le Bail, C. Louvet, D. Hendler, F. de Braud, C. Wilson, F. Morvan, A. Bonetti, *J. Clin. Oncol.* **2000**, *18*, 2938.
[6] J. Y. Douillard, S. Siena, J. Cassidy, J. Tabernero, R. Burkes, M. Barugel, Y. Humblet, G. Bodoky, D. Cunningham, J. Jassem, F. Rivera, I. Kocakova, P. Ruff, M. Blasinska-Morawiec, M. Smakal, J. L. Canon, M. Rother, K. S. Oliner, M. Wolf, J. Gansert, *J. Clin. Oncol.* **2010**, *28*, 4697.
[7] H. Hurwitz, L. Fehrenbacher, W. Novotny, T. Cartwright, J. Hainsworth, W. Heim, J. Berlin, A. Baron, S. Griffing, E. Holmgren, N. Ferrara, G. Fyfe, B. Rogers, R. Ross, F. Kabbinavar, *N. Engl. J. Med.* **2004**, *350*, 2335.
[8] M. Peeters, T. J. Price, A. Cervantes, A. F. Sobrero, M. Ducreux, Y. Hotko, T. Andre, E. Chan, F. Lordick, C. J. A. Punt, A. H. Strickland, G. Wilson, T. E. Ciuleanu, L. Roman, E. Van Cutsem, V. Tzekova, S. Collins, K. S. Oliner, A. Rong, J. Gansert, *J. Clin. Oncol.* **2010**, *28*, 4706.
[9] L. B. Saltz, S. Clarke, E. Diaz-Rubio, W. Scheithauer, A. Figer, R. Wong, S. Koski, M. Lichinitser, T. S. Yang, F. Rivera, F. Couture, F. Sirzen, J. Cassidy, *J. Clin. Oncol.* **2008**, *26*, 2013.
[10] E. Van Cutsem, C. H. Kohne, E. Hitre, J. Zaluski, C. R. C. Chien, A. Makhson, G. D'Haens, T. Pinter, R. Lim, G. Bodoky, J. K. Roh, G. Folprecht, P. Ruff, C. Stroh, S. Tejpar, M. Schlichting, J. Nippgen, P. Rougier, *N. Engl. J. Med.* **2009**, *360*, 1408.
[11] M. S. Edwards, S. D. Chadda, Z. Zhao, B. L. Barber, D. P. Sykes, *Colorectal Dis.* **2012**, *14*, e31.
[12] J. L. Grem, N. Harold, J. Shapiro, D. Q. Bi, M. G. Quinn, S. Zentko, B. Keith, J. M. Hamilton, B. P. Monahan, S. Donavan, F. Grollman, G. Morrison, C. H. Takimoto, *J. Clin. Oncol.* **2000**, *18*, 3952.
[13] L. Kelland, *Nat. Rev. Cancer* **2007**, *7*, 573.
[14] L. B. Saltz, J. V. Cox, C. Blanke, L. S. Rosen, L. Fehrenbacher, M. J. Moore, J. A. Maroun, S. P. Ackland, P. K. Locker, N. Pirotta, G. L. Elfring, L. L. Miller, I. S. Group, *N. Engl. J. Med.* **2000**, *343*, 905.
[15] T. Andre, C. Boni, L. Mounedji-Boudiaf, M. Navarro, J. Tabernero, T. Hickish, C. Topham, M. Zaninelli, P. Clingan, J. Bridgewater, I. Tabah-Fisch, A. de Gramont, M. Investigators, *N. Engl. J. Med.* **2004**, *350*, 2343.
[16] F. Kabbinavar, H. I. Hurwitz, L. Fehrenbacher, N. J. Meropol, W. F. Novotny, G. Lieberman, S. Griffing, E. Bergsland, *J. Clin. Oncol.* **2003**, *21*, 60.
[17] V. T. Devita, Jr, T. Lawrence, S. A. Rosenberg, *Cancer: Principles and Practice of Oncology: Annual Advances in Oncology*. Lippincott Williams & Wilkins, Philadelphia, PA **2012**.
[18] C. Gravalos, J. Cassinello, I. Fernandez-Ranada, E. Holgado, *Clin. Colorectal Cancer* **2007**, *6*, 691.
[19] A. Arora, E. M. Scholar, *J. Pharmacol. Exp. Ther.* **2005**, *315*, 971.
[20] S. L. Moulder, B. S. Craft, G. N. Hortobagyi, *Anti-Cancer Agents Med. Chem.* **2008**, *8*, 481.
[21] K. Suda, H. Mizuuchi, Y. Maehara, T. Mitsudomi, *Cancer Metastasis Rev.* **2012**, *31*, 807.
[22] L. Lin, T. G. Bivona, *Chemother. Res. Pract.* **2012**, *2012*, 817297.
[23] C. Ozvegy-Laczka, J. Cserepes, N. B. Elkind, B. Sarkadi, *Drug Resist. Updates* **2005**, *8*, 15.
[24] P. K. Kreeger, D. A. Lauffenburger, *Carcinogenesis* **2010**, *31*, 2.

[25] A. Leber, R. Hontecillas, V. Abedi, N. Tubau-Juni, V. Zoccoli-Rodriguez, C. Stewart, J. Bassaganya-Riera, *Artif. Intell. Med.***2017**, *78*, 1.
[26] C. Lee, Z. Luo, K. Y. Ngiam, M. Zhang, K. Zheng, G. Chen, B. C. Ooi, W. L. J. Yip, *Big Healthcare Data Analytics: Challenges and Applications*, Springer International Publishing, Cham, Switzerland **2017**.
[27] R. M. Weinshilboum, L. Wang, *Mayo Clin. Proc.* **2017**, *92*, 1711.
[28] J. Weisner, I. Landel, C. Reintjes, N. Uhlenbrock, M. Trajkovic-Arsic, N. Dienstbier, J. Hardick, S. Ladigan, M. Lindemann, S. Smith, L. Quambusch, R. Scheinpflug, L. Depta, R. Gontla, A. Unger, H. Müller, M. Baumann, C. Schultz-Fademrecht, G. Günther, A. Maghnouj, M. P. Müller, M. Pohl, C. Teschendorf, H. Wolters, R. Viebahn, A. Tannapfel, W. Uhl, J. G. Hengstler, S. A. Hahn, J. T. Siveke, D. Rauh, *Cancer Res.* **2019**, *79*, 2367.
[29] A. Zimmer, A. Tendler, I. Katzir, A. Mayo, U. Alon, *PLoS Biol.* **2017**, *15*, 2002518.
[30] J. B. Fitzgerald, B. Schoeberl, U. B. Nielsen, P. K. Sorger, *Nat. Chem. Biol.* **2006**, *2*, 458.
[31] A. Tendler, A. Zimmer, A. Mayo, U. Alon, *PLoS Comput. Biol.* **2019**, *15*, e1006956.
[32] I. Katzir, M. Cokol, B. B. Aldridge, U. Alon, *PLoS Comput. Biol.* **2019**, *15*, e1006774.
[33] B. Kim, H. B. Pang, J. Kang, J. H. Park, E. Ruoslahti, M. J. Sailor, *Nat. Commun.* **2018**, *9*, 1969.
[34] R. Liu, L. Zhang, J. Zhao, Z. Luo, Y. Huang, S. Zhao, *Adv. Ther.* **2018**, *1*, 1800041.
[35] H. Meng, A. E. Nel, *Adv. Drug Delivery Rev.* **2018**, *130*, 50.
[36] M. Ziegler, X. Xu, M. L. Yap, H. Hu, J. Zhang, K. Peter, *Adv. Ther.* **2019**, *2*, 1800133.
[37] F. C. Lam, S. W. Morton, J. Wyckoff, T. L. Vu Han, M. K. Hwang, A. Maffa, E. Balkanska-Sinclair, M. B. Yaffe, S. R. Floyd, P. T. Hammond, *Nat. Commun.* **2018**, *9*, 1991.
[38] A. Weiss, X. T. Ding, J. R. van Beijnum, I. Wong, T. J. Wong, R. H. Berndsen, O. Dormond, M. Dallinga, L. Shen, R. O. Schlingemann, R. Pili, C. M. Ho, P. J. Dyson, H. van den Bergh, A. W. Griffioen, P. Nowak-Sliwinska, *Angiogenesis* **2015**, *18*, 233.
[39] F.-C. Chang, S. L. Levengood, N. Cho, L. Chen, E. Wang, J. S. Yu, M. Zhang, *Adv. Ther.* **2018**, *1*, 1800058.
[40] E. L. Diamond, B. H. Durham, G. A. Ulaner, E. Drill, J. Buthorn, M. Ki, L. Bitner, H. Cho, R. J. Young, J. H. Francis, R. Rampal, M. Lacouture, L. A. Brody, N. Ozkaya, A. Dogan, N. Rosen, A. Iasonos, O. Abdel-Wahab, D. M. Hyman, *Nature* **2019**, *567*, 521.
[41] R. Sano, K. Krytska, C. E. Larmour, P. Raman, D. Martinez, G. F. Ligon, J. S. Lillquist, U. Cucchi, P. Orsini, S. Rizzi, B. R. Pawel, D. Alvarado, Y. P. Mosse, *Sci. Transl. Med.* **2019**, *11*, eaau9732.
[42] K. Chakraborty, C. Dutta, S. Mukherjee, A. Biswas, P. Gayen, G. George, S. Raghothama, S. Ghosh, S. Dey, D. Bhattacharyya, R. Sinha Roy, *Adv. Ther.* **2018**, *1*, 1800018.
[43] E. C. A. Nyns, R. H. Poelma, L. Volkers, J. J. Plomp, C. I. Bart, A. M. Kip, T. J. van Brakel, K. Zeppenfeld, M. J. Schalij, G. Q. Zhang, A. A. F. de Vries, D. A. Pijnappels, *Sci. Transl. Med.* **2019**, *11*, eaau6447.
[44] L. J. Eggermont, R. Hammink, K. G. Blank, A. E. Rowan, J. Tel, C. G. Figdor, *Adv. Ther.* **2018**, *1*, 1800021.
[45] P. K. Wong, F. Q. Yu, A. Shahangian, G. H. Cheng, R. Sun, C. M. Ho, *Proc. Natl. Acad. Sci. USA.* **2008**, *105*, 5105.
[46] A. Zarrinpar, D. K. Lee, A. Silva, N. Datta, T. Kee, C. Eriksen, K. Weigle, V. Agopian, F. Kaldas, D. Farmer, S. E. Wang, R. Busuttil, C. M. Ho, D. Ho, *Sci. Transl. Med.* **2016**, *8*, 333ra49.
[47] T. Kee, C. Weiyan, A. Blasiak, P. Wang, J. K. Chong, J. Chen, B. T. T. Yeo, D. Ho, C. L. Asplund, *Adv. Ther.* **2019**, *2*, 1900023.
[48] B. E. Bejnordi, M. Veta, P. J. van Diest, B. van Ginneken, N. Karssemeijer, G. Litjens, J. A. W. M. van der Laak, C. Consortium, *JAMA, J. Am. Med. Assoc.* **2017**, *318*, 2199.
[49] Y. Chen, E. Argentinis, G. Weber, *Clin. Ther.* **2016**, *38*, 688.
[50] R. Harpaz, W. DuMouchel, M. Schuemie, O. Bodenreider, C. Friedman, E. Horvitz, A. Ripple, A. Sorbello, R. W. White, R. Winnenburg, N. H. Shah, *J. Biomed. Inf.* **2017**, *76*, 41.
[51] R. C. Cai, M. Liu, Y. Hu, B. L. Melton, M. E. Matheny, H. Xu, L. Duan, L. R. Waitman, *Artif. Intell. Med.* **2017**, *76*, 7.
[52] J. Haefeli, A. R. Ferguson, D. Bingham, A. Orr, S. J. Won, T. I. Lam, J. Shi, S. Hawley, J. L. Liu, R. A. Swanson, S. M. Massa, *Sci. Rep.* **2017**, *7*, 42474.
[53] J. H. Chen, S. M. Asch, *N. Engl. J. Med.* **2017**, *376*, 2507.
[54] I. Al-Shyoukh, F. Q. Yu, J. Y. Feng, K. R. Yan, S. Dubinett, C. M. Ho, J. S. Shamma, R. Sun, *BMC Syst. Biol.* **2011**, *5*, 88.
[55] A. Silva, B. Y. Lee, D. L. Clemens, T. Kee, X. T. Ding, C. M. Ho, M. A. Horwitz, *Proc. Natl. Acad. Sci. USA.* **2016**, *113*, E2172.
[56] B. Y. Lee, D. L. Clemens, A. Silva, B. J. Dillon, S. Maslesa-Galic, S. Nava, X. T. Ding, C. M. Ho, M. A. Horwitz, *Nat. Commun.* **2017**, *8*, 1038.
[57] A. J. Pantuck, D.-K. Lee, T. Kee, P. Wang, S. Lakhotia, M. H. Silverman, C. Mathis, A. Drakaki, A. S. Belldegrun, C.-M. Ho, D. Ho, *Adv. Ther.* **2018**, *1*, 1800104.
[58] M. B. M. A. Rashid, T. B. Toh, L. Hooi, A. Silva, Y. Z. Zhang, P. F. Tan, A. L. Teh, N. Karnani, S. Jha, C. M. Ho, W. J. Chng, D. Ho, E. K. H. Chow, *Sci. Transl. Med.* **2018**, *10*, eaan0941.
[59] A. Weiss, R. H. Berndsen, X. T. Ding, C. M. Ho, P. J. Dyson, H. van den Bergh, A. W. Griffioen, P. Nowak-Sliwinska, *Sci. Rep.* **2015**, *5*, 14508.
[60] X. T. Ding, W. J. Liu, A. Weiss, Y. Y. Li, I. Wong, A. W. Griffioen, H. van den Bergh, H. Q. Xu, P. Nowak-Sliwinska, C. M. Ho, *Phys. Biol.* **2014**, *11*, 065003.
[61] S. Chakradhar, *Nat. Med.* **2017**, *23*, 1244.
[62] D. A. Ho, C. H. K. Wang, E. K. H. Chow, *Sci. Adv.* **2015**, *1*, e1500447.
[63] G. M. Huang, Y. Sun, X. Ge, X. Wan, C. B. Li, *World J. Gastroenterol.* **2015**, *21*, 6194.
[64] E. L. Kwak, Y. J. Bang, D. R. Camidge, A. T. Shaw, B. Solomon, R. G. Maki, S. H. Ou, B. J. Dezube, P. A. Janne, D. B. Costa, M. Varella-Garcia, W. H. Kim, T. J. Lynch, P. Fidias, H. Stubbs, J. A. Engelman, L. V. Sequist, W. Tan, L. Gandhi, M. Mino-Kenudson, G. C. Wei, S. M. Shreeve, M. J. Ratain, J. Settleman, J. G. Christensen, D. A. Haber, K. Wilner, R. Salgia, G. I. Shapiro, J. W. Clark, A. J. Iafrate, *N. Engl. J. Med.* **2010**, *363*, 1693.
[65] V. DeVita, Jr, T. S. Lawrence, S. A. Rosenberg, *DeVita, Hellman, and Rosenberg's Cancer: Principles and Practice of Oncology*, Wolters Kluwer, Philadelphia, PN **2014**.
[66] H. Q. Xu, J. Jaynes, X. T. Ding, *Stat. Sinica* **2014**, *24*, 269.
[67] M. B. M. A. Rashid, T. B. Toh, L. Hooi, A. Silva, Y. Zhang, P. F. Tan, A. L. Teh, N. Karnani, S. Jha, C.-M. Ho, W. J. Chng, D. Ho, E. K.-H. Chow, *Sci. Transl. Med.* **2018**, *10*, eaan0941.

